INVESTIGATION OF STRAUS-2 PULSED ELECTRON ACCELERATOR CHARACTERISTICS

V.S. Gordeev, G.A. Myskov, V.O. Filippov, V.Ya. Averchenkov
VNIIEF, Sarov, Russia

Last years a successful development of high-voltage pulse forming techniques based on stepped transmission lines led to creation of a set of powerful and compact electrophysics facilities including a high-current pulsed electron accelerator STRAUS-2 [1, 2]. The first sample of this accelerator was started up into exploitation in 1989. At present, three facilities of the same type exist in VNIIEF, one of them is used as an injector for a linear induction accelerator LIA-10M [2-5]. Two others are autonomous and applied for research in radiation physics.

STRAUS-2 accelerator (Fig. 1a) is designed by a scheme of five-cascade double stepped forming line – DSFL (Fig. 1b), that allows to realize a high voltage transformation factor: when charging the accelerator's DSFL up to 0.63 MV the idle voltage pulse amplitude reaches 4.1 MV on its output.

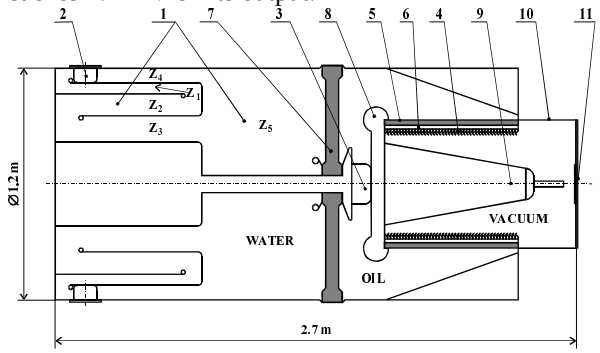

1 – DSFL; 2 – multichannel switch; 3 – pre-pulse switch; 4 – sectioned isolator; 5 – polyethylene tube; 6 - electrolyte layer; 7 – water–oil separating diaphragm; 8 – shielding electrode; 9 – cathode holder with a cathode; 10 – output vacuum chamber; 11 - anode flange with a target unit.

a)

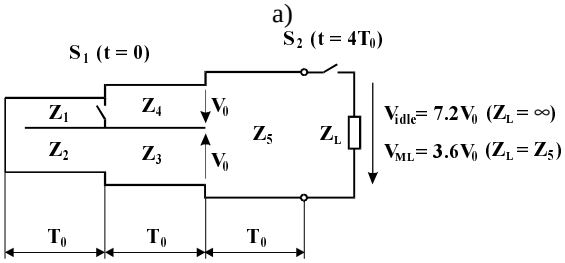

Z_1=0.8 Ohm; Z_2=1.9 Ohm; Z_3=3.2 Ohm; Z_4=0.9 Ohm; Z_5=18 Ohm;
T_0≈20 ns.

b)

Fig. 1. Sketch of STRAUS-2 accelerator (a) and an electric circuit of its DSFL (b).

The output voltage, current and pulse duration can be varied, but most often the follow operating mode is realized: V~3 MV, I~50 kA, τ_p~20÷40 ns (FWHM), that corresponds to maximum dose parameters at accelerator operating in the X-ray generation mode. In this case the diode configuration is used as follows: graphite cathode ∅30÷40 mm having two coaxial ring edges, accelerating gap – $\Delta_{A\text{-}C}$~50 mm, target unit – 0.5 mm of tantalum and 10 mm of aluminum (as a filter). The target is chosen some thicker than optimal for enlarging its operation resource (100÷150 pulses). Below the characteristics are given for X-ray radiation produced by the STRAUS-2 accelerator [1, 5].

Dose (Si):	at the output flange	100 Gy
	at 1 m from the target	0.2 Gy
Dose power:	at the output flange	$5\cdot10^9$ Gy/s
	at 1 m from the target	$1\cdot10^7$ Gy/s
X-ray radiation pulse width:		15÷25 ns
Irradiation spot diameter (D_{max}/D_{min}=2):	at the output flange	8 cm
	at 1 m from the target	80 cm

The dose remains practically unchangeable within the X-ray pulse duration 15÷25 ns (FWHM), but the dose power has a maximum at τ_p~15 ns. The dose constancy is provided for account of some growth (~10÷15 %) of the diode current and voltage, observed at pulse width reduction. Out of the above-mentioned range the dose falls because of the diode voltage and current decrease. In case of τ_p>25ns it occurs due to arrival time mismatching of partial electromagnetic waves, forming the output pulse, to the diode load. At τ_p<15 ns the X-ray radiation pulse is formed at the falling part of the accelerating pulse. Notice, that the dose parameters can be risen by ~1.5 times through increasing the DSFL charging voltage up to the maximum value 0.7 MV along with decreasing the target thickness up to 0.25÷0.3 mm. At that, however, resource characteristics of the accelerator will be some below.

In Fig. 2 the X-ray radiation pulse shape and the energy spectrum of photons generated by the STRAUS-2 accelerator are shown. The spectrum was calculated, being based on the experimentally measured curve of the photon flux attenuation in plumbum, with a method of minimization of directed divergence. The measured photon fluence near the accelerator axis at 2.5 m from the target is about $6.1\cdot10^9$ cm^{-2}. At the photon boundary energy 2.8 MeV a maximum of the spectrum distribution lies near 0.55 MeV, and the mean energy of quanta is about 0.73 MeV. The RMS error of the calculations does not exceed ±6% overall the spectrum besides its lower boundary, where it reaches ±15%. In the field <0.1 MeV the spectrum was not specified, because this energy range lay under the sensitivity threshold of the radiation detectors (SCD1-01) used for the measurements.

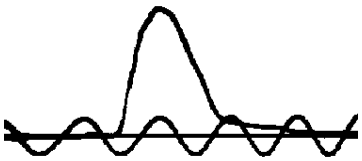

Time label frequency - 25 MHz

a)

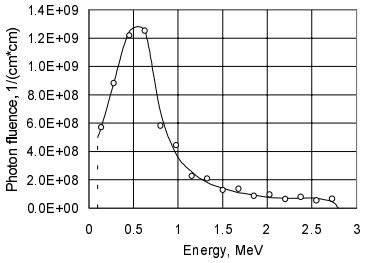

b)

Fig. 2. X-ray radiation pulse shape (a) and the photon energy spectrum (b) of STRAUS-2 accelerator.

For output of the electron beam ($j_e \leq 10$ kA/cm^2) into atmosphere a window ∅180 mm is used, that consist of two 0.1 mm thickness titanium foils placed at 15 mm distance each from other. Only the external foil is hermetic, while the internal one provides the constancy of diode geometry, as it is not deformed at vacuum pumping. In such configuration the energy and current losses are less than 10%. Leaving the diode electrons undergo strong deceleration in the electric field of the self beam space charge, that is illustrated by Fig. 3, where, for comparison, the relative dose distributions of electron beam in aluminum and in air are given. In aluminum, where the space charge is compensated, at the boundary electron energy ~3 MeV their radiation length is ~1.5 g/cm^2. In air this value is ≤0.2 g/cm^2. The cross section dimensions of the beam grow significantly, too. For example, at 1 m distance from the output window the beam increases its diameter from 4 cm to ~30 cm.

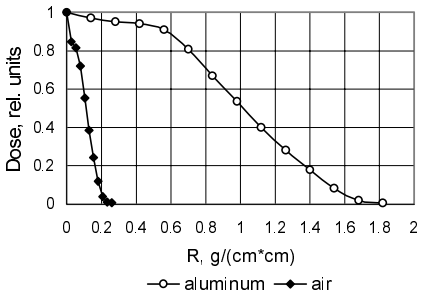

Fig. 3. Relative dose distributions in aluminum and in air for the electron beam of STRAUS-2 accelerator.

For some applications electron beam focusing mode are of interest to form a spot of a small diameter at the target, what allows using the STRAUS-2 accelerator as a near-point X-ray source. In this case a focusing unit on the base of vacuum conic transmission line with a self-magnetic insulation (MITL) is joined to the accelerator output (Fig. 4). The length of this line is about 25 cm, and its wave impedance is approximately 90 Ohm. As a prototype it was used a scheme realized in a PULSERAD-1480 accelerator [6]. The focusing unit configuration was optimized on results of numeric calculations for electron flow in the MITL and in the diode with the electromagnetic code KARAT [7]. The inner electrode of the MITL is a cone with a half-angle ~10° and it is a constructive prolongation of the accelerator cathode holder. A half-angle of the outer conic electrode of the MITL is about 45°. The cathode is made of Wo-Ni-Fe alloy. It is also cone with a flat or annular face edge of 4÷15 mm diameter. The anode is flat with a diameter ~100 mm. The target is a tantalum disk ∅30 mm (working part of 20 mm diameter) and of 0.3 mm thickness. Behind the target an aluminum filter of 15 mm thickness is placed. The accelerating gap can be varied within 5÷20 mm by choice of a cathode of corresponding length.

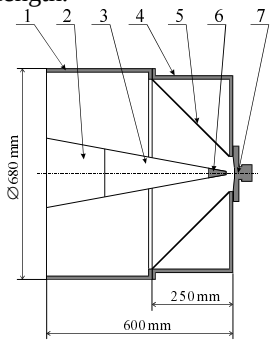

Fig. 4. Sketch of the focusing unit: 1 – vacuum chamber; 2 – cathode holder; 3 – inner MITL electrode; 4 – focusing unit case; 5 – outer MITL electrode; 6 - cathode; 7 – anode flange with a target unit.

During a pulse the target suffered a significant thermomechanic effect of the beam and plasma being formed in the diode, because of that its working part was entirely destroyed (Fig. 5a). There was also observed melting the central part of aluminum filter up to 5÷6 mm depth. The quality of beam focusing was evaluated on its X-ray images obtained with an obscure chamber (Fig. 5b). With the same purpose in a number of pulses it was used a target of 1 mm thickness instead of 0.3 mm one, affecting an electron beam on that did not cause its entire destruction but only perforation its central part (Fig. 5b). At that, the diameter of the formed hole corresponded rather well to the mean beam diameter on the target. However, in this case the X-ray generation efficiency was lowered by ~30÷50% depending on the accelerating gap.

t_t=0.3 mm t_t=1mm

a)

$\Delta_{A\text{-}C}$=5 mm $\Delta_{A\text{-}C}$=15 mm $\Delta_{A\text{-}C}$=20 mm

b)

Fig. 5. Target fotos (a, scale 1:2) and X-ray images of the beam (b, scale 1:1).

Beam focusing was provided at $\Delta_{A\text{-}C} \leq 20$ mm, and the best results were achieved at the current pulse duration $\tau_{0,5}$=45 ns being maximal for the STRAUS-2 accelerator. At $\Delta_{A\text{-}C}$>20 mm beam focusing was disturbed due to the change of MITL operation mode, as the diode impedance became higher than the effective MITL impedance. In this case the MITL voltage and current practically did not change with the accelerating gap growth (fig. 6) and became equal to 2.85 MV and 42 kA corresponding to the self-consistent operation mode of the MITL (line-dominated mode). At that, the electron flow was absent on the target but was closed on the MITL outer (anode) electrode surface.

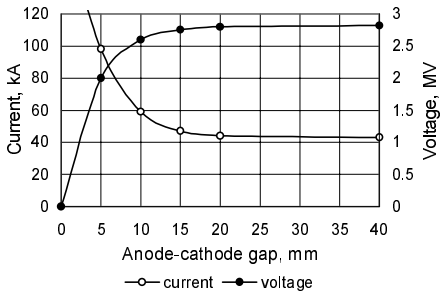

Fig. 6. Diode voltage and current versus the anode-cathode gap.

In Fig. 7 there are shown X-ray intensity distributions in the focused spot on the target at different anode-cathode gap. At growth of the gap $\Delta_{A\text{-}C}$ from 5 to 20 mm the average spot diameter weakly increases from 4.5 to 6 mm. Simultaneously a redistribution of radiation intensity occurs in the spot from its center to periphery. The radiation dose grows and reaches the maximum at $\Delta_{A\text{-}C}$=15 mm: ~0,12 Gy (Si) at 1 m distance from the target. At that, the focused spot has the diameter about 5 mm. Beam pinching on the target under the influence of the self-magnetic field (~5÷8 T) lead to some deterioration of its angular characteristics. This is most noticeable at $\Delta_{A\text{-}C} \leq 10$ mm and it is revealed as the characteristic dose drop near r=0 on the curve of transverse dose distribution at 1 m from the target (Fig. 8). It is interesting to note that in this mode the dose inhomogeneity in the irradiation spot of ~0,6 m diameter (at 1 m from the target) is ≤±15%, that is twice less than in a usual irradiating mode.

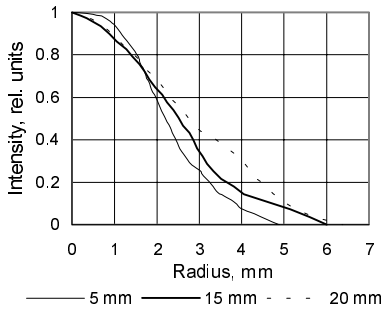

Fig. 7. Relative distributions of X-ray radiation intensity in the focused spot at different accelerating gap.

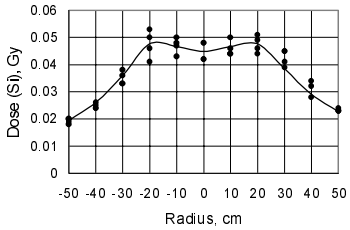

Fig. 8. Transverse dose distribution of X-ray radiation at 1 m from the target ($\Delta_{A\text{-}C}$=10 mm, t_t=1 mm).

At present time a lot of experimental data was obtained at the STRAUS-2 accelerator, being of practical interest in view of its application for research in radiation physics, pulsed radiography and other spheres. Furthermore, this data were used for verifying and testing of simulation methods, algorithms and codes applied for calculations in a designing process of similar type facilities as the STRAUS-2 accelerator.

REFERENCES

1. V.S. Bossamykin, V.S. Gordeev, A.I. Pavlovskii et al. STRAUS-2 Electron Pulsed Accelerator. Proc. 9th Int. Pulsed Power Conf., Albuquerque, NM, 1993, pp. 910-912.
2. V.S. Bossamykin, V.S. Gordeev, A.I. Pavlovskii et al. Pulsed Power Electron Accelerators with the Forming Systems Based on Stepped Transmission Lines. Proc. 9th Int. Conf. on High Power Particle Beams (BEAMS-92), Washington, DC, 1992, vol. 1, pp. 505-510.
3. V.S. Gordeev, V.S. Bossamykin, A.I. Pavlovskii et al. Linear Induction Accelerator LIA-10M. Proc. 9th Int. Pulsed Power Conf., Albuquerque, NM, 1993, pp. 905-907.
4. V.S. Bossamykin, V.S. Gordeev V.F.Basmanov et al. VANT, 1997, N. 4-5 (31-32), p 117 - 119.
5. V.S. Bossamykin, V.S. Gordeev V.F.Basmanov et al. VANT, 1997, N. 4-5 (31-32), p 120 – 122.
6. V.P. Tarakanov. User Manual for Code KARAT. BRA Inc., USA, 1992.
7. P. Champney, P. Spence. PULSERAD 1480 – a 9 MV Pulsed Electron Accelerator with an Intensely Focused Beam. IEEE Trans. Nucl. Sc., Vol. NS-22, No. 3, June 1975.